Journal Pre-proof

Quantitative Volumetric Analysis of Retinal Ischemia with an Oxygen Diffusion Model and Optical Coherence Tomography Angiography

Pengxiao Zang, PhD, Tristan T. Hormel, PhD, Thomas S. Hwang, MD, Yali Jia, PhD

PII: S2666-9145(24)00115-5

DOI: https://doi.org/10.1016/j.xops.2024.100579

Reference: XOPS 100579

To appear in: *Ophthalmology Science*

Received Date: 18 January 2024

Revised Date: 5 April 2024

Accepted Date: 1 July 2024

Please cite this article as: Zang P., Hormel T.T., Hwang T.S. & Jia Y., Quantitative Volumetric Analysis of Retinal Ischemia with an Oxygen Diffusion Model and Optical Coherence Tomography Angiography, *Ophthalmology Science* (2024), doi: https://doi.org/10.1016/j.xops.2024.100579.

Quantitative Volumetric Analysis of Retinal Ischemia with an Oxygen Diffusion Model and Optical Coherence Tomography Angiography

Pengxiao Zang, PhD,[1] Tristan T. Hormel, PhD,[1] Thomas S. Hwang, MD,[1] Yali Jia, PhD[1, 2]

Meeting Presentation: Association for Research in Vision and Ophthalmology Imaging in the Eye Conference, 2023.

Financial Support: This work was supported by the National Institute of Health (R01 EY027833, R01 EY035410, R01 EY024544, R01EY036429, R01 EY031394, T32 EY023211, UL1TR002369, P30 EY010572); the Malcolm M. Marquis, MD Endowed Fund for Innovation; an Unrestricted Departmental Funding Grant and Dr. H. James and Carole Free Catalyst Award from Research to Prevent Blindness (NewYork, NY); Edward N. & Della L. Thome Memorial Foundation Award; and the Bright Focus Foundation (G2020168, M20230081). The sponsor or funding organization had no role in the design or conduct of this research.

Conflict of Interest: Oregon Health & Science University (OHSU) and Dr. Yali Jia have a significant financial interest in Optovue/Visionix, Inc. Genentech, Inc. and Optos, Inc. These potential conflicts of interest have been reviewed and managed by OHSU.

Running head: 3D quantitative analysis of retinal ischemia

Address for reprints: 515 SW Campus Dr., CEI 3154, Portland, Oregon 97239-4197

Key words: Retinal ischemia, oxygen distribution, optical coherence tomography angiography, diabetic retinopathy.

Abbreviations and Acronyms: AUC = area under receiver operating characteristic curve; DCP = deep capillary plexus; DME = diabetic macular edema; DR = diabetic retinopathy; ETDRS = Early Treatment of Diabetic Retinopathy Study; FAZ = foveal avascular zone; ICP = intermediate capillary plexus; nDR = diabetic without diabetic retinopathy; NPA = nonperfusion area; nrDR = non-referable diabetic retinopathy; OCT = optical coherence tomography; OCTA = optical coherence tomography angiography; r_nvtDR = referable but non-vision threatening diabetic retinopathy; SVC = superficial vascular complex; vtDR = vision threatening diabetic retinopathy.

1. Casey Eye Institute, Oregon Health & Science University, Portland, OR, USA
2. Department of Biomedical Engineering, Oregon Health & Science University, Portland, OR, USA

Correspondence: Yali Jia, PhD, Casey Eye Institute & Department of Biomedical Engineering, Oregon Health & Science University, 515 SW Campus Dr., CEI 3154, Portland, Oregon 97239-4197. E-mail: jiaya@ohsu.edu

Abstract

Purpose: Retinal ischemia is a major feature of diabetic retinopathy (DR). Traditional nonperfused areas measured by optical coherence tomography angiography (OCTA) measure blood supply but not ischemia. We propose a novel 3-dimensional (3D) quantitative method to derive ischemia measurements from OCTA data.

Design: Cross-sectional study.

Participants: We acquired 223 macular OCTA volumes from 33 healthy eyes, 33 diabetic eyes without retinopathy, 7 eyes with non-referable DR, 17 eyes with referable but non-vision-threatening DR, and 133 eyes with vision-threatening DR.

Methods: Each eye was scanned using a spectral-domain OCTA system (Avanti RTVue-XR, Visionix/Optovue, Inc) with 1.6 mm scan depth in a 3 × 3-mm region (640 × 304 × 304 voxels) centered on the fovea. For each scanned OCTA volume, a custom algorithm removed flow projection artifacts. We then enhanced, binarized, and skeletonized the vasculature in each OCTA volume and generated a 3D oxygen tension map using a zero-order kinetics oxygen diffusion model. Each volume was scaled to the average retina thickness in healthy controls after foveal registration and flattening of the Bruch membrane. Finally, we extracted 3D ischemia maps by comparison with a reference map established from scans of healthy eyes using the same processing. To assess the ability of the ischemia maps to grade DR severity, we constructed receiver-operating characteristic (ROC) curves for diagnosing diabetes, referable DR, and vision-threatening DR.

Main outcome measures: Spearman correlation coefficient and area under ROC curve (AUC) were used to quantify the ability of the ischemia maps to DR.

Results: The ischemia maps showed that the ischemic tissues were at or near pathologically non-perfused areas, but not the normally non-vascular tissue, such as the foveal avascular zone. We found multiple novel metrics, including inferred 3D-oxygen tension, ischemia index, and ischemic volume ratio, were strongly correlated with DR severity. The AUCs of ischemia index measured were 0.95 for diabetes, 0.89 for DR, 0.88 for referable DR, and 0.85 for vision threatening DR.

Conclusions: A quantitative method to infer 3D oxygen tension and ischemia using OCTA in diabetic eyes can identify ischemic tissue that are more specific to pathologic changes in DR.

Introduction

DR is a leading cause of preventable blindness globally [1]. Early detection of this disease is crucial for successful treatment outcomes [2-4]. Retinal ischemia is a key feature of DR that drives the downstream complications, making it an important pathology to characterize [5, 6]. The current OCTA-based methods to assess ischemia have focused on vessel density and nonperfusion areas (NPA), both of which measure the absence of vessels without reference to normal [7-10]. However, nonperfusion can be physiologic, as in the foveal avascular zone (FAZ).

More importantly, these measures of nonperfusion do not directly measure ischemia, which implies inadequate blood flow of any given tissue. A true measure of ischemia would require the knowledge of metabolic demand and diffusion of oxygen at a point. Without observing frank tissue abnormalities, such as opacification of the retina in arterial occlusions, it is impossible to measure the imbalance between the metabolic demand and oxygen supply. Currently, the direct measurements of retinal tissue oxygen and ischemia are mostly based on microelectrodes and fluorescence lifetime imaging ophthalmoscopy which can measure oxygen concentration or partial oxygen pressure on animal models [11, 12]. But they could not be used on living human eyes. In addition, the visible light OCT can generate optical imaging of oximetry and has a potential of working on living human eyes. But the generated optical imaging is only the measurement of vascular oximetry, not the oxygen tension within the retinal tissue [13]. It is worth noting that one can estimate normal perfusion at any given point of the retina based on the spatial relationship between tissue and blood vessels in the normal retina. By comparing the spatial relationship between vessels and tissue against the reference created by averaging of the retina from normal eyes, we propose a model that indirectly measures ischemia, not just nonperfusion. We hypothesize that this method will more reliably detect ischemic changes in diabetic retinopathy compared to measurements of nonperfusion, while avoiding detection of pathology in normally avascular areas, such as the foveal avascular zone.

To obtain an indirect estimate of ischemic regions, volumetric anatomic information should be supplemented with oxygen diffusion dynamics in order to better infer tissue oxygen saturation. Therefore, to detect ischemia, we propose combining vascular anatomic measurements from OCTA with an oxygen diffusion model.

Methods

Data acquisition

We included healthy controls and diabetic patients with DR severity ranging from no clinically evident retinopathy to proliferative diabetic retinopathy. One or both eyes of each participant underwent 7-field color fundus photography and an OCTA scan using a commercial 70-kHz spectral-domain OCT (SD-OCT) system (RTVue-XR Avanti, Optovue/Visionix Inc.) with 840-nm central wavelength. The scan depth was 1.6 mm in a 3 × 3-mm region (640 × 304 × 304 voxels) centered on the fovea. Two repeated B-frames were captured at each cross-sectional location. Structural images were obtained by averaging the two repeated and registered B-frames. Blood flow was detected using the split-spectrum amplitude-decorrelation angiography (SSADA) algorithm [14]. For each volume, two continuously acquired raster scans (one x-fast scan and one y-fast scan) were registered and merged with an orthogonal registration algorithm to reduce motion artifacts [15]. In addition, a projection-resolved OCTA algorithm was applied to all OCTA scans to remove flow projection artifacts [16]. Scans with a signal strength index (SSI) lower than 50 were excluded.

To quantitatively analyze the oxygen tension and ischemia maps across different DR severities, a masked trained retina specialist (TSH) graded 7-field color fundus photographs based on Early Treatment of Diabetic Retinopathy Study (ETDRS) scale [17, 18]. The presence of DME was determined using the central subfield thickness from structural OCT based on the Diabetic Retinopathy Clinical Research Network (DRCR.net) standard [19]. DR severity was defined as non-referable (nrDR) when the ETDRS level was better than 35 and without DME; referable but non-vision threatening DR (r_nvtDR) when ETDRS level was between 35-47 without DME; and vision threatening DR (vtDR) when ETDRS level 53 or worse or any stage of DR with DME [20]. Participants were enrolled after informed consent in accordance with an Institutional Review Board approved protocol. This study complied with the Declaration of Helsinki and the Health Insurance Portability and Accountability Act.

Framework summary

Our 3D oxygen tension and ischemia quantitative analysis framework includes several steps (Fig. 1).

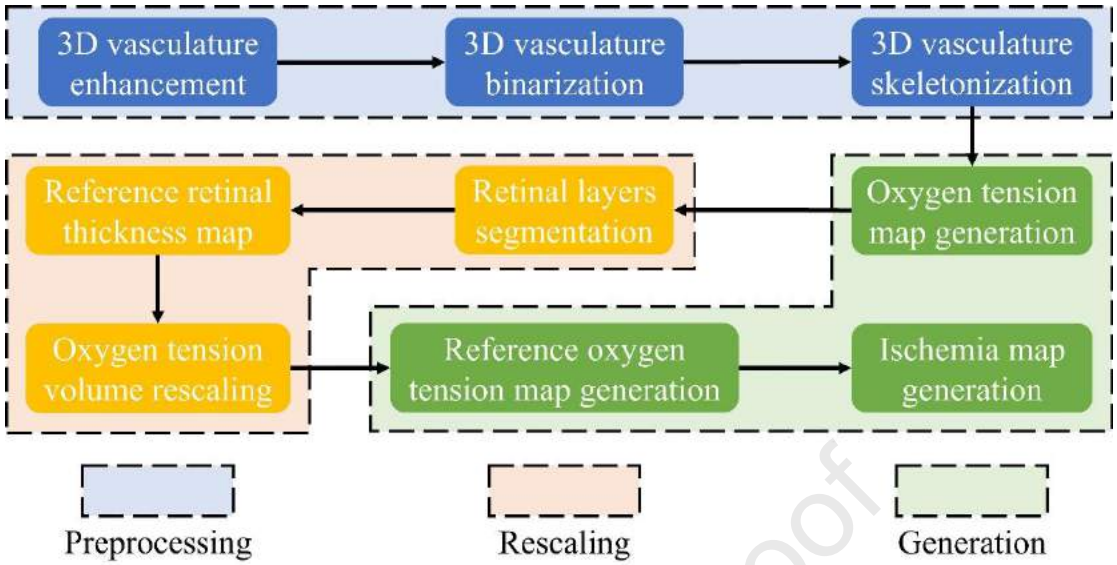

Fig. 1. The framework of the proposed 3D quantitative method for oxygen tension and ischemia of OCTA volume. In preprocessing (blue boxes), we first volumetrically enhanced, binarized, and skeletonized the vasculature. The oxygen tension map was then calculated based on the skeletonized volume using an oxygen diffusion model (green box on the second line). We next rescaled each oxygen tension map based on a reference thickness map, which was the average of all healthy controls (yellow boxes). Finally, the ischemia map was generated by comparison with a reference oxygen tension map established by combining half of the healthy volumes (bottom two green boxes).

Data preprocessing

To improve the computational efficiency, a sub-volume from the inner limiting membrane (ILM) to the bottom of Bruch's membrane (BM) plus 20 voxels (including choriocapillaris) was extracted from each original OCTA volume. In preprocessing, the vasculature in both the retina and choroid of each sub-volume was enhanced using the optimally oriented flux method [21, 22]. The enhanced vasculature was then binarized using an empirically selected threshold of the mean plus 0.1 standard deviations of the non-zero voxels. The binary images were then skeletonized using a medial axis transform algorithm [23, 24].

Oxygen diffusion calculation

An oxygen diffusion model with zero-order kinetics (Fig. 2) was used to generate a convolutional kernel K to apply to the skeletonized OCTA volumes in order to generate an oxygen tension map [25] according to

$$K = \begin{cases} \left(1 - \frac{d}{L_p}\right)^2 \text{ for } 0 \le d \le L_\text{p} \\ 0 \text{ for x} > L_\text{p} \end{cases} \quad (1)$$

where d is the distance from the voxel being acted on by the kernel and L_p is the penetration depth given by

$$L_p = \sqrt{2D_t\alpha_t P/M} \quad (2)$$

where D_t is the oxygen diffusion coefficient 1.97×10^{-5} cm^2/s in tissue [26], α_t is the solubility coefficient 2.4×10^{-5} mL O^2/mL tissue/mmHg [27], P is oxygen tension in the target vessel [11], and M is retinal tissue oxygen consumption [11]. To get a L_p close to the real value, P and M were respectively selected as the oxygen tension of retinal arteries 101 mmHg and average retinal tissue oxygen consumption 1.8 ml O^2/100 g tissue/min measured from Long-Evans rat in light adaptation [11]. In addition, we have assumed equal oxygen tension within the vessels and homogenous consumption throughout the retina.

To transfer L_p from millimeters to voxels, each skeletonized OCTA volume was resized to isotropic resolution before the oxygen diffusion calculation. Oxygen tension maps T are then obtained by convolving the established kernels with the skeletonized vasculatures

$$T = V * K \quad (3)$$

where $*$ is the convolution operation, V are the set of vascular voxels, and K was the generated convolutional kernel.

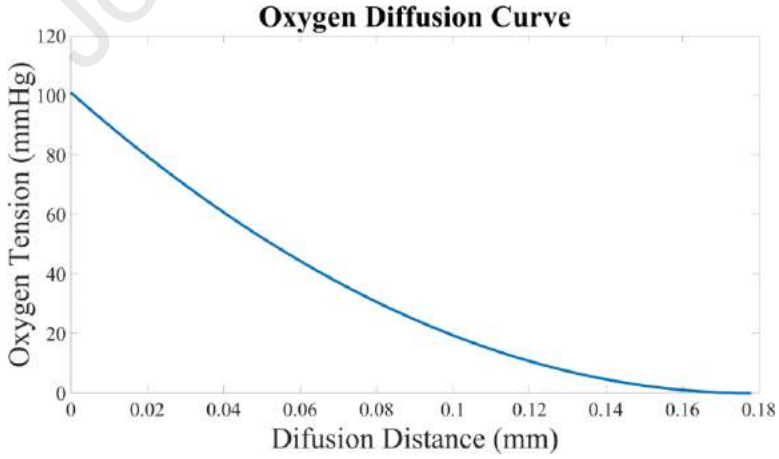

Fig. 2. The oxygen diffusion curve for vessels in the retina and choroidal using the parameters described in the main text.

Retina rescaling

After the generation of oxygen tension volume, the thickness of each retinal layer in the volume was rescaled based on a reference thickness map. To obtain the reference thickness map, we first calculated a thickness map based on the commercial software in the SD-OCT system in this study (RTVue-XR Avanti, Optovue/Visionix Inc.). In addition, for the cases with severe pathologies, the automated layer segmentation was manually corrected by graders using our COOL-ART software [28, 29]. The following retinal layers or boundaries were involved in the generation of the thickness map: the ILM, nerve fiber layer (NFL), ganglion cell layer (GCL), inner plexiform layer (IPL), inner nuclear layer (INL), outer plexiform layer (OPL), outer nuclear layer (ONL), ellipsoid zone (EZ), retinal pigment epithelium (RPE), and BM (Fig. 3). A reference thickness map was constructed by averaging the thickness of each retinal layer of all the healthy cases after foveal registration and BM flattening. To obtain the rescaled volumes, we registered individual scans to the reference thickness map by centering each on the fovea. The fovea was detected as the center of the binary mask of the FAZ, which was segmented using an empirically selected threshold on the combined image of inner retinal *en face* OCTA projection and thickness map. Each retinal layer was then rescaled using linear interpolation based on the thickness of the corresponding layer in the reference thickness map (Fig. 3).

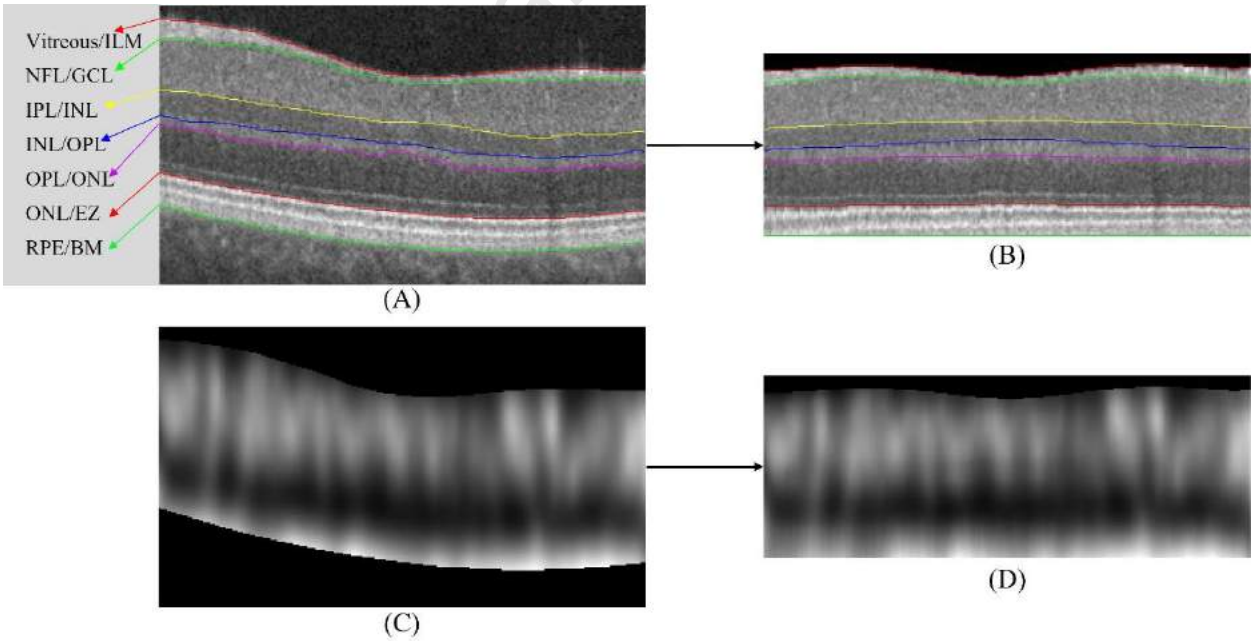

Fig. 3. Rescaling based on retinal thickness to obtain a reference volume. For each retinal layer, each A-line was rescaled using linear interpolation based on the thickness of the same layer at the same *en face* position. (A) The segmented six retinal layers based on the seven marked boundaries in the original B-scan before rescaling. (B) The rescaled and flattened (based on RPE/BM)

B-scan from (A). Each retinal layer was rescaled to the exact same shape of the reference thickness map. (C) The B-scan oxygen tension with the same position of (A). (D) The rescaled B-scan oxygen tension from (C) using the rescaling shown from (A) to (B).

Ischemia map generation

After all the oxygen tension maps were rescaled, all the healthy maps were split to a development set with 17 volumes and a testing set with 16 volumes. Oxygen tension maps T_{min} and T_{sigma} were then respectively generated as the minimum and mean minus 2.5 times standard deviation among all the maps in the development set (4). The reference map T_{ref} was then generated as the maximum between T_{min} and T_{sigma}. The ischemia map of each OCTA volume could be finally generated as

$$T_{\mathrm{ref}} = T_{\mathrm{min}} - 2.5 \times T_{\mathrm{sigma}}$$
$$M = \frac{\mathrm{Max}(T_{\mathrm{ref}} - T,\ 0)}{T_{\mathrm{ref}}} \quad (4)$$

where *M* is the generated ischemia map, and T is the oxygen tension map of the corresponding case. In addition, the testing set and maps of other DR severities were only used to evaluate the generated reference oxygen tension map.

Ischemia quantification

Before the quantification of ischemia, it was important to clarify that the voxel values in the generated oxygen tension maps could only estimate the relative differences in the distribution of oxygen tension and do not represent the actual oxygen tension values in the corresponding eye. To ensure that the estimated oxygen tensions fall within the actual oxygen tension values range, they were normalized by dividing them by the target vessel oxygen tension *P* = 101 mmHg [11]. To quantitatively analyze the generated ischemia map which was generated based on the normalized oxygen tension map, we defined two ischemia metrics. The first metric was the ischemia index, defined as the percentage of oxygen tension loss compared to the oxygen tension in the reference map (calculated using Eq. 4). The ischemia index could be calculated for each voxel in the ischemia map. The second metric was the ischemic volume ratio, defined as the percentage of ischemic voxels compared to the total volume of the retina. The ischemic volume ratio could be calculated for each volumetric ischemia map.

Evaluation on different retinal layers

To analyze the 3D oxygen tension and ischemia maps on different retinal layers, three retinal capillary plexus layers, the superficial vascular complex (SVC), intermediate capillary plexus (ICP), and deep capillary plexus (DCP) were selected [7, 30, 31]. The SVC was defined as the inner 80% of the ganglion cell complex (GCC), which included all structures between the ILM and IPL/INL border. The ICP was defined as the outer 20% of the GCC and the inner 50% of the INL. The DCP was defined as the remaining slab internal to the outer boundary of the OPL (Fig. 3) [29]. The average *en face* projections of the 3D oxygen tension and ischemia maps were generated on three selected retinal layers for both qualitative and quantitative analysis. Additionally, the generated *en face* projections could be also used to compare with traditional nonperfusion maps which were generated on the same retinal layers based on previously developed models in our group [32-34].

Results

We recruited and examined 20 healthy participants and 179 patients with diabetes at the Casey Eye Institute, Oregon Health & Science University in the United States. The data characteristics are shown below (Table 1).

Table 1. Data distribution and characteristic

Severity	Healthy	nDR	nrDR	r_nvtDR	vtDR
Volume number	33	33	7	17	133
Age, mean (SD), y	37.9 (12.3)	54.1 (15.7)	45.3 (15.1)	60.5 (11.3)	58.7 (12.2)
Female, %	54.8%	48.5%	71.4%	64.7%	51.1%
SSI, mean (SD)	78.2 (7.7)	69.9 (7.5)	75.7 (7.3)	68.5 (7.7)	66.4 (7.1)

DR = diabetic retinopathy; nDR = diabetic without DR; nrDR = non-referable DR; r_nvtDR = referable but non-vision-threatening DR; vtDR = vision-threatening DR; SSI = signal strength index.

Qualitative analysis

Compared to the segmented NPA, which focused on the capillary dropout [30], our ischemia map attempts to focus on retinal tissues that lacked oxygen supply by modeling diffusion dynamics. We firstly compare the generated 3D ischemia maps with segmented NPA maps in three healthy eyes. Notably, the *en face* projections of the 3D ischemia maps did not highlight the FAZ, which, in contrast, was segmented as NPAs (Fig. 4). Additionally, the ischemia maps highlighted much smaller areas compared to the NPA maps in these three healthy eyes. On the other hand, the ischemia map of a vision-threatening DR eye clearly shows 3D ischemic regions (Fig. 5). In this example, the highlighted ischemic regions appeared similarly to the pathological NPAs (Fig. 5D). By overlaying the B-scan oxygen tension map and OCTA (Fig. 5E), we could examine how the ischemia volumes were distributed in cross-sectional view; therefore, the ischemic regions can be revealed volumetrically (Fig. 5F).

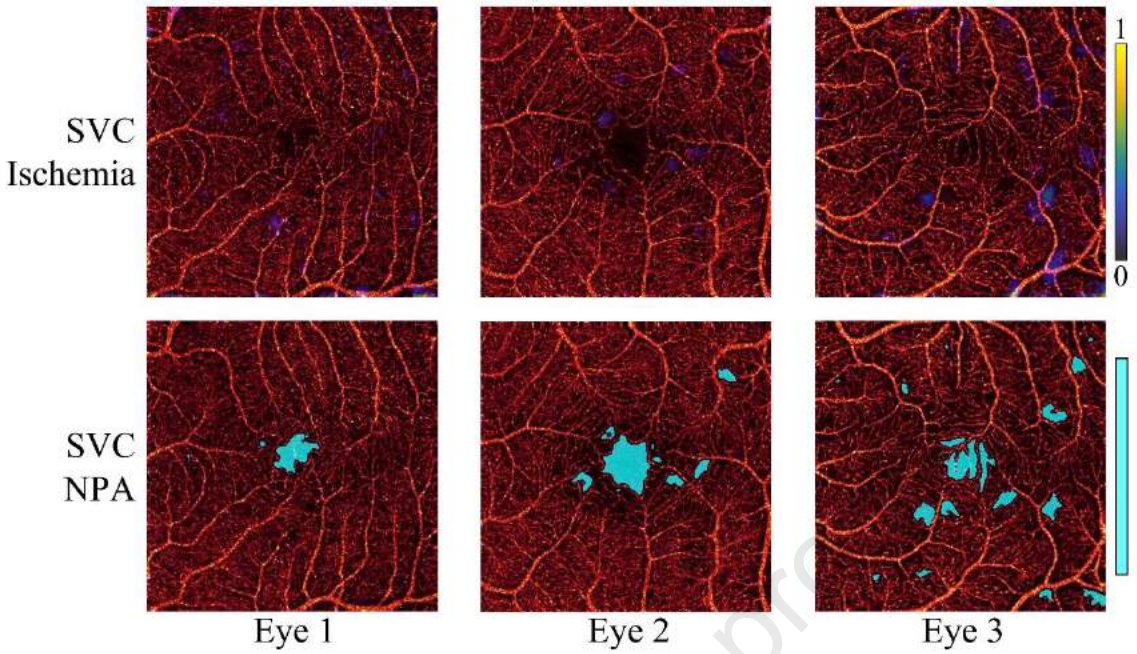

211

212 Fig. 4. Generated 3D ischemia map of three healthy eyes in the testing set. The mean projection of superficial vascular complex
213 (SVC) from each ischemia map was calculated and overlayed on the corresponding OCTA *en face* image. Compared to the
214 segmented non-perfusion area (NPA) [32], the ischemia map did not identify every region that lacked vessels, instead
215 highlighting regions with poor inferred oxygen concentration. That the ischemia map avoided detecting non-pathological
216 capillary drop out (e.g. in the foveal avascular zone) suggests that it may be a more sensitive indicator of pathology than NPA
217 measurements.

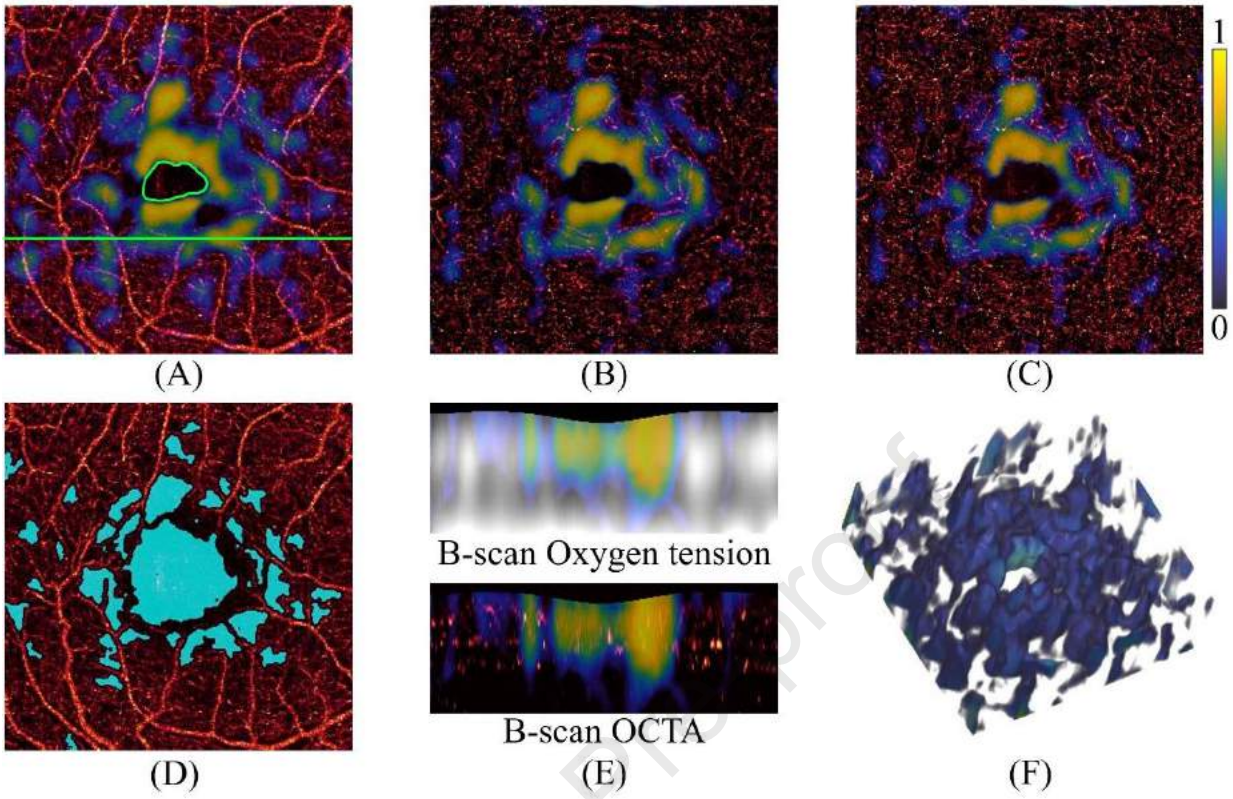

Fig. 5. Generated 3D ischemia map of a vision threatening diabetic retinopathy (DR) OCTA volume, showing the ischemia distribution in different retinal layers. The ischemic areas broadly match the non-perfusion area (NPA), but avoid the foveal avascular zone. (A) *En face* superficial vascular complex (SVC) projection of the ischemia map overlayed on an *en face* OCTA image of the SVC. The healthy avascular tissue was demarcated with a green boundary. (B) *En face* intermediate capillary plexus (ICP) projection of the ischemia map. (C) *En face* deep capillary plexus (DCP) projection of the ischemia map. (D) Segmented non-perfusion area overlayed on the SVC [32]. The non-perfusion areas appear similar to the ischemic areas, with the exception of the FAZ. (E) A B-scan ischemia map overlayed on the B-scan oxygen tension and OCTA image marked by a green line in (A). (F) 3D view of the ischemia volumes.

Quantitative analysis

To analyze the correlations between the generated 3D ischemia maps and DR severity, we calculated the average oxygen tension, average ischemia index, and ischemic volume ratio for the OCTA volumes in each DR severity (Table 2, Fig. 6). For the 5 DR severities examined, lower oxygen tension, higher ischemia index, and ischemic volume ratio showed strong correlations with increased DR severity (Table 2; Spearman correlation coefficients). In

addition, compared to the ischemic volume ratio, the ischemia index achieved a higher area under the receiver operating characteristic curve (AUC) for diagnosing DR, rDR and vtDR (Table 3).

Table 2. The correlations between three ischemia metrics (Mean ± Std) and DR severities

Mean ± Std	Numbers	Oxygen tension	Ischemic volume ratio	Ischemia index
Healthy	16	56.75 ± 2.48	8.56% ± 3.96%	1.12% ± 0.65%
nDR	33	52.86 ± 3.43	16.99% ± 7.87%	2.73% ± 2.09%
nrDR	7	50.43 ± 5.04	23.55% ± 12.01%	3.71% ± 2.99%
r_nvtDR	17	50.07 ± 5.27	26.60% ± 12.82%	4.99% ± 3.31%
vtDR	133	47.63 ± 5.64	33.77% ± 13.20%	7.96% ± 5.02%
Spearman correlation coefficient along severities (P-values)		-0.49*	0.58*	0.50*

DR = diabetic retinopathy; nDR = diabetic without DR; nrDR = non-referable DR; r_nvtDR = referable but non-vision-threatening DR; vtDR = vision-threatening DR; *p-value < 0.001.

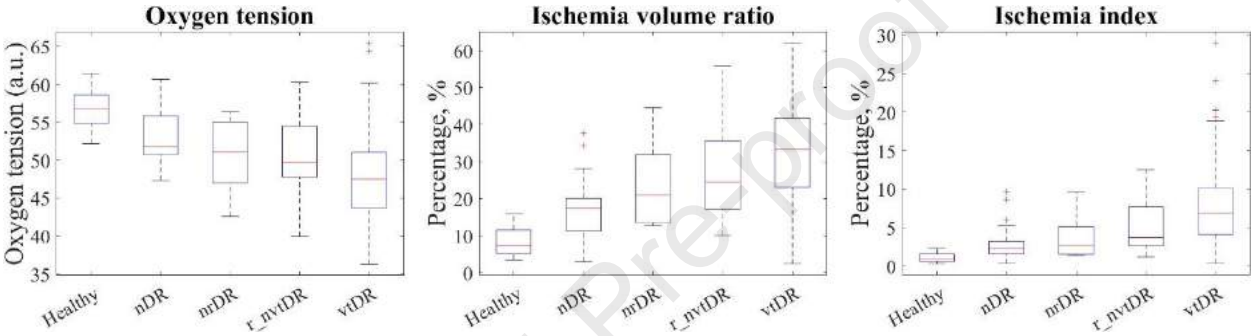

Fig. 6. Boxplots based on average oxygen tensions, ischemic volume ratio, and ischemia index of 5 different diabetic retinopathy (DR) severities: healthy, diabetic without DR (nDR), non-referable DR (nrDR), referable but non vision threatening DR (r_nvtDR), and vision threatening DR (vtDR). For both ischemic volume ratio and index, the median values (red lines in the middle and right figures) were positively correlated with DR severity. For the oxygen tensions, the median values (red lines in the left figure) were negatively correlated with DR severity.

Table 3. AUCs of three ischemia metrics on diagnosing DR with variant severities

	Oxygen tension	Ischemic volume ratio	Ischemia index
Diabetes	0.10	**0.95**	0.94
DR	0.18	0.89	**0.89**
rDR	0.19	0.87	**0.88**
vtDR	0.22	0.83	**0.85**

DR = diabetic retinopathy; rDR = referable DR; vtDR = vision -threatening DR; AUC = area under receiver operating characteristic curve.

Plexus-specific analysis and the comparison to NPAs

To evaluate whether ischemia metrics perform better in the plexus-specific slabs, we analyzed Spearman correlation coefficient and AUC for each retinal plexus (Table S4 and S5). We found that the ICP had the highest oxygen tension among all DR severities (Table S4). The SVC had the highest ischemic volume ratio and ischemia index and achieved the highest AUC for diabetes diagnosis compared to ICP and DCP (Table S5). The DCP achieved the

highest AUC in discriminating different levels of DR compared to SVC and ICP (Table S5). However, the ischemia biomarkers using the whole retina achieved higher diagnostic performances than individual plexuses in all severities (Table 3).

To verify whether our oxygen tension and ischemia maps correlated with the capillary dropout, the Spearman correlation coefficients between the mean NPAs and oxygen tension and ischemia maps were calculated (Table S6). The mean oxygen tensions and NPAs were negatively correlated. The ischemic volume ratios and mean indexes were positively correlated with the NPA. The high correlations shown in Table S6 demonstrate our method could correctly reflect the oxygen tension and ischemia changes due to capillary dropout.

Discussion

In this study, we proposed a 3D quantitative analysis method to estimate oxygen tension and ischemia in OCTA volumes of subjects with different DR severities. We generated oxygen tension and ischemia maps based on 3D microvasculatures in OCTA volumes. Unlike current nonperfusion detection methods, our ischemia maps highlighted only pathologic changes that result in lower oxygen levels while ignoring normal avascular tissue, such as in the FAZ. To the best of our knowledge, our method is the first 3D analysis method for both oxygen tension and ischemia based on OCTA volume.

Our method used an oxygen diffusion model with zero-order kinetics to generate the oxygen tension map based on enhanced and skeletonized vessels. For model parameters, we used values measured from Long-Evans rats in light adaptation in the oxygen diffusion model [11]. While some parameters, such as oxygen tension in vessels or consumption in the retina, likely vary with location, assessing local variation directly is difficult. We instead chose a simpler model to determine ischemic locations by using values from the literature rather than fit values for model parameters. This approach avoids over-fitting the data and ensures the results are reasonable. In addition, our model produced reasonable oxygen tension values in the healthy avascular regions; the estimated oxygen tension values in the outer retina within and outside the FAZ were similar.

The other key aspect of our approach is the reference map. To generate this reference map, we performed two crucial procedures to make it more objective. First, we used skeletonized vasculatures to prevent the varied distributions of large vessels present in different healthy volumes from influencing the oxygen tension distribution in

the reference map. Second, we separated the healthy controls into a development set and a testing set and only used the development set to establish the reference map. This approach allowed verification of the reliability of our results.

Compared to current OCTA-based nonperfusion analysis methods [7-10], our method has three major technical advantages. First, our oxygen tension map was generated by combining a physical model with real-world measurements. This contrasts with conventional image processing kernels, which are empirically determined and do not incorporate physiological information. By including measurements from physiologic models, the model is more than a mathematical construct but a physical modeling of oxygen tension. Second, we generated the ischemia map by comparing it with a reference oxygen tension map. As a result, our generated map focused only on the retinal tissues with oxygen levels lower than normal and disregarded the normal avascular tissue (Fig. 4). Finally, our ischemia maps were generated volumetrically, preserving the three-dimensionality of interaction between perfusion and tissue in the retina. Unlike NPA segmentation, ischemia should be quantified as a volumetric entity, not in separate plexuses. This could also explain why the ischemia biomarkers using the whole retina achieved higher diagnostic performances compared to individual plexuses in all severities.

These ischemia-based metrics have two potential clinical advantages. Because they specifically identify pathologic changes, they may be more accurate when used as a screening tool across population variation. The variation in foveal avascular zone size has been widely reported [35, 36]. Less is known about variations in avascular zones near larger vessels. An objective and quantitative metric that is specific to vascular damage from diabetes can potentially improve on the current photography-based screening, and even incremental improvement in accuracy can have a large impact on the efficiency of screening. Secondly, by directing clinician attention to the ischemic, and not physiologically avascular areas, it has the potential of providing clinicians with more accurate insight about the severity and localization of the disease.

This study had several limitations. First, a longitudinal study is needed to establish causality of the proposed model. Second, the model did not consider the differences between arteries and veins, large vessels and microvasculature, and the retina and choroid. It is likely that these differences affect our model parameters. In addition, the reference oxygen tension map was generated only based on 17 healthy controls. In future studies, we plan to use a larger number of eyes scanned from a more diverse population for the reference volume and allow parameters to vary in

different vessels. Lastly, the model parameters were measured from animal studies but not human eyes. This shortcoming can be potentially compensated by integrating our current method with a visible light OCTA system to calculate the oxygen tension maps based on the measured oximetry in different vessels, thereby enhancing the accuracy of our oxygen tension map [13, 37].

Conclusion

We proposed a 3D quantitative analysis method for the oxygen tension and ischemia of eyes with or without DR. The 3D oxygen tension and ischemia maps were generated using an oxygen diffusion model with zero-order kinetics based on skeletonized vasculature in OCTA volume. Lower oxygen tension, higher ischemia index, ischemic volume ratio from the model were strongly correlated with increased DR severity. The ischemia maps did not identify normal avascular tissue as ischemic tissue. Our method offers a 3D quantitative analysis of oxygen tension and retinal ischemia in diabetic retinopathy. The generated oxygen tension and ischemic maps could be used in future studies of retinal oxygen supply reduction caused by DR or other eye diseases.

Reference

1. Wilkinson CP, Ferris III FL, Klein RE, et al. Proposed international clinical diabetic retinopathy and diabetic macular edema disease severity scales. *Ophthalmology.* 2003;110(9):1677-1682.
2. Bragge P, Gruen RL, Chau M, et al. Screening for presence or absence of diabetic retinopathy: a metaanalysis. *Arch Ophthalmol.*, 2011;129(4):435–444.
3. Hazin R, Colyer M, Lum F, Barazi MK. Revisiting diabetes 2000: challenges in establishing nationwide diabetic retinopathy prevention programs. *Am. J. Ophthalmology.*, 2011;152(5):723–729.
4. National Health Services Diabetic Eye Screening Programme of the United Kingdom. *National Health Service Diabetic Retinopathy Programme Annual Report, April 2007-March 2008*. Gloucester, England: National Health Services Diabetic Eye Screening Programme of the United Kingdom (2008).
5. Early Treatment Diabetic Retinopathy Study Research Group. Fluorescein angiographic risk factors for progression of diabetic retinopathy: ETDRS report number 13. *Ophthalmology*. 1991;98:834–840.
6. Early Treatment Diabetic Retinopathy Study Research Group. Classification of diabetic retinopathy from fluorescein angiograms: ETDRS report number 11. *Ophthalmology*. 1991;98:807–822.

7. Zhang M, Hwang TS, Dongye C, Wilson DJ, Huang D, Jia Y. Automated quantification of nonperfusion in three retinal plexuses using projection-resolved optical coherence tomogra phy angiography in diabetic retinopathy. *Invest Ophthalmol Vis Sci*. 2016;57:5101–5106.
8. Hwang TS, Gao SS, Liu L, et al. Automated quantification of capillary nonperfusion using optical coherence tomography angiography in diabetic retinopathy. *JAMA Ophthalmol*. 2016;134:367–373.
9. Schottenhamml J, Moult EM, Ploner S, et al. An automatic, intercapillary area-based algorithm for quantifying diabetes-related capillary dropout using optical coherence tomography angiography. *Retina*. 2016;36(suppl 1):S93–S101.
10. Lauermann P, Oterendrop CV, Storch MW et al. Distance-Thresholded intercapillary area analysis versus vessel-based approaches to quantify retinal ischemia in OCTA. *Transl. Vis. Sci. Technol*. 2019;8(4):28-28.
11. Lau JCM, Linsenmeier RA. Oxygen consumption and distribution in the Long-Evans rat retina. *Experimental eye research*. 2012;102:50-58.
12. Dysli C, et al. Fluorescence lifetime imaging ophthalmoscopy. *Progress in retinal and eye research*. 2017;60:120-143.
13. Pi S, Hormel TT, Wei X, et al. Retinal capillary oximetry with visible light optical coherence tomography. *Proceedings of the National Academy of Sciences*. 2020;117(21):11658-11666.
14. Jia Y, Tan O, Tokayer J, et al. Split-spectrum amplitude-decorrelation angiography with optical coherence tomography. *Opt. Express*. 2012;20(4):4710–4725.
15. Kraus MF, Liu JJ, Schottenhamml J, et al. Quantitative 3D-OCT motion correction with tilt and illumination correction, robust similarity measure and regularization. *Biomed. Opt. Express*. 2014;5(8):2591–2613.
16. Wang J, Zhang M, Hwang TS, et al. Reflectance-based projection resolved optical coherence tomography. *Biomed. Opt. Express*. 2017;8(3):1536-1548.
17. Early Treatment Diabetic Retinopathy Study Research Group. Fundus photographic risk factors for progression of diabetic retinopathy: ETDRS report number 12. *Ophthalmology*. 1991;98(5):823-833.
18. Ophthalmoscopy D, Levels E. International clinical diabetic retinopathy disease severity scale detailed table. 2002.

19. Flaxel CJ, Adelman RA, Bailey ST, et al. Diabetic retinopathy preferred practice pattern®. *Ophthalmology*. 2020;127(1):66-145.
20. Wong TY, Sun J, Kawasaki R, et al. Guidelines on diabetic eye care: the international council of ophthalmology recommendations for screening, follow-up, referral, and treatment based on resource settings. *Ophthalmology*. 2018;125(10):1608-1622.
21. Law MWK, Albert CSC. Three dimensional curvilinear structure detection using optimally oriented flux. *Computer Vision–ECCV 2008: 10th European Conference on Computer Vision, Marseille, France, October 12-18, 2008, Proceedings, Part IV 10*. Springer Berlin Heidelberg, 2008.
22. Law MWK, Tay K, Leung A, Garvin GJ, Li S. Dilated divergence based scale-space representation for curve analysis. *European Conference on Computer Vision*. Springer, Berlin, Heidelberg, 2012.
23. Lee T, Kashyap RL, Chu C. Building skeleton models via 3-D medial surface/axis thinning algorithms. *CVGIP: Graphical Models and Image Processing*. 1994;56(6):462-478.
24. Kerschnitzki M, Kollmannsberger P, Burghammer M. et al. Architecture of the osteocyte network correlates with bone material quality. *Journal of Bone and Mineral Research*. 2013;28(8):1837-1845.
25. Popel AS. Theory of oxygen transport to tissue. *Critical reviews in biomedical engineering.* 1989;17(3):257.
26. RoH HD, Goldstick TK, Linsenmeier RA. Spatial variation of the local tissue oxygen diffusion coefficient measured in situ in the cat retina and cornea. *Oxygen Transport to Tissue*. 1990;127-136.
27. Linsenmeier RA, Braun RD. Oxygen distribution and consumption in the cat retina during normoxia and hypoxemia. *The Journal of general physiology*. 1992;99:177-197.
28. Zhang M, Wang J, Pechauer AD, et al. Advanced image processing for optical coherence tomographic angiography of macular diseases. *Biomed. Opt. Express*. 2015;6(12):4661–4675.
29. Guo Y, Camino A, Zhang M, et al. Automated segmentation of retinal layer boundaries and capillary plexuses in wide-field optical coherence tomographic angiography. *Biomed. Opt. Express*. 2018;9(9):4429-4442.
30. Hormel TT, Wang J, Bailey ST, Hwang TS, Huang D, Jia Y. Maximum value projection produces better en face OCT angiograms than mean value projection. *Biomed. Opt. Express*. 2018;9(12):6412-6424.

31. Campbell JP, Zhang M, Hwang TS, et al. Detailed vascular anatomy of the human retina by projection-resolved optical coherence tomography angiography. *Sci. Rep.* 2017;7:42201.
32. Wang J, Hormel TT, You Q et al. Robust non-perfusion area detection in three retinal plexuses using convolutional neural network in OCT angiography. *Biomed. Opt. Express*. 2020;11(1);330-345.
33. Guo Y, Camino A, Wang J, Huang D, Hwang TS, Jia Y. MEDnet, a neural network for automated detection of avascular area in OCT angiography. *Biomed. Opt. Express*. 2018;9(11):5147-5158.
34. Guo Y, Hormel TT, Xiong H, et al. Development and validation of a deep learning algorithm for distinguishing the nonperfusion area from signal reduction artifacts on OCT angiography. *Biomed. Opt. Express*. 2019;10(7):3257-3268.
35. Giocanti-Aurégan A, Gazeau G, Hrarat L, et al. Ethnic differences in normal retinal capillary density and foveal avascular zone measurements. *International Ophthalmology*. 2020;40:3043-3048.
36. Laotaweerungsawat S, Psaras C, Haq Z, Liu X, Stewart JM. Racial and ethnic differences in foveal avascular zone in diabetic and nondiabetic eyes revealed by optical coherence tomography angiography. *PLoS One*. 2021;16(10):e0258848.
37. Song W, Shao W, Yi W, et al. Visible light optical coherence tomography angiography (vis-OCTA) facilitates local microvascular oximetry in the human retina. *Biomedical Optics Express*. 2020;11(7):4037-4051.

Table 1. Data distribution and characteristic

Severity	Healthy	nDR	nrDR	r_nvtDR	vtDR
Volume number	33	33	7	17	133
Age, mean (SD), y	37.9 (12.3)	54.1 (15.7)	45.3 (15.1)	60.5 (11.3)	58.7 (12.2)
Female, %	54.8%	48.5%	71.4%	64.7%	51.1%
SSI, mean (SD)	78.2 (7.7)	69.9 (7.5)	75.7 (7.3)	68.5 (7.7)	66.4 (7.1)

DR = diabetic retinopathy; nDR = diabetic without DR; nrDR = non-referable DR; r_nvtDR = referable but non-vision-threatening DR; vtDR = vision-threatening DR; SSI = signal strength index.

Table 2. The correlations between three ischemia metrics (Mean ± Std) and DR severities

Mean ± Std	Numbers	Oxygen tension	Ischemic volume ratio	Ischemia index
Healthy	16	56.75 ± 2.48	8.56% ± 3.96%	1.12% ± 0.65%
nDR	33	52.86 ± 3.43	16.99% ± 7.87%	2.73% ± 2.09%
nrDR	7	50.43 ± 5.04	23.55% ± 12.01%	3.71% ± 2.99%
r_nvtDR	17	50.07 ± 5.27	26.60% ± 12.82%	4.99% ± 3.31%
vtDR	133	47.63 ± 5.64	33.77% ± 13.20%	7.96% ± 5.02%
Spearman correlation coefficient along severities (P-values)		-0.49*	0.58*	0.50*

DR = diabetic retinopathy; nDR = diabetic without DR; nrDR = non-referable DR; r_nvtDR = referable but non-vision-threatening DR; vtDR = vision-threatening DR; *p-value < 0.001.

Table 3. AUCs of three ischemia metrics on diagnosing DR with variant severities

	Oxygen tension	Ischemic volume ratio	Ischemia index
Diabetes	0.10	**0.95**	0.94
DR	0.18	0.89	**0.89**
rDR	0.19	0.87	**0.88**
vtDR	0.22	0.83	**0.85**

DR = diabetic retinopathy; rDR = referable DR; vtDR = vision-threatening DR; AUC = area under receiver operating characteristic curve.

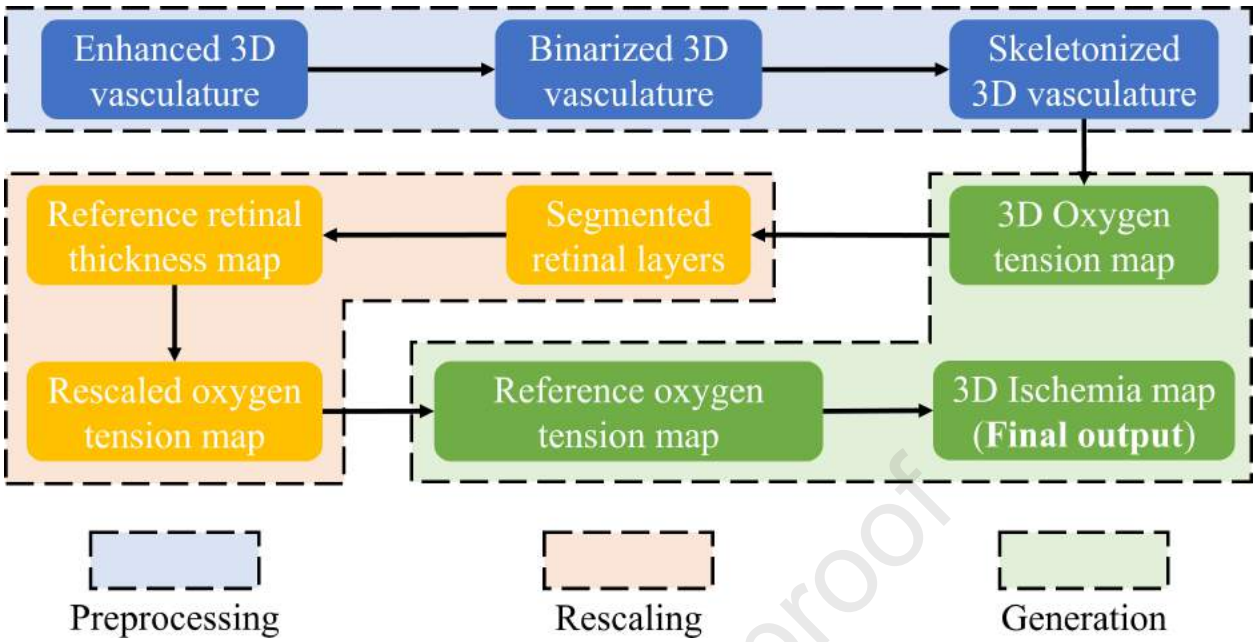

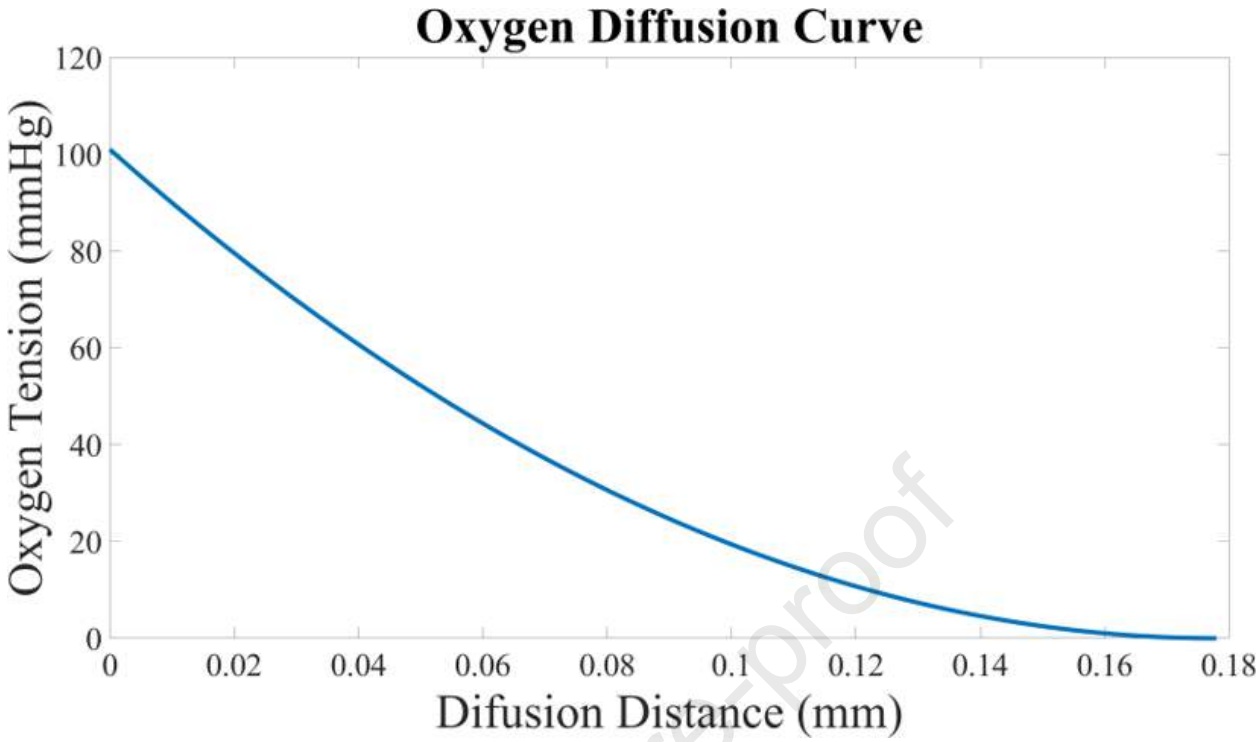

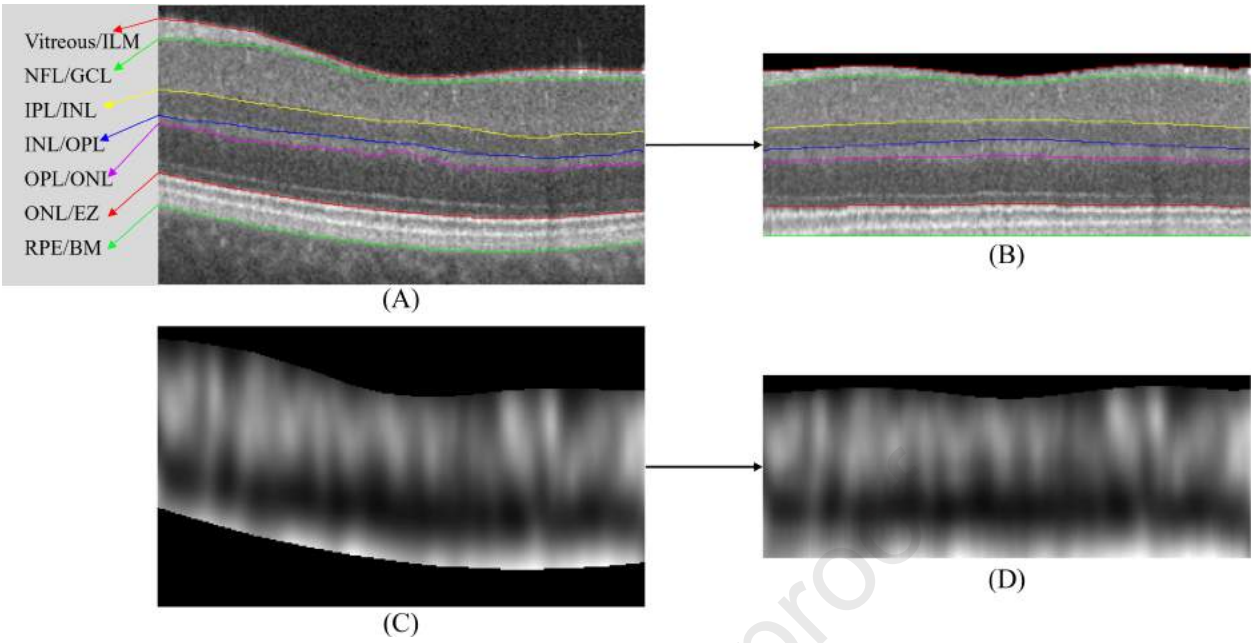

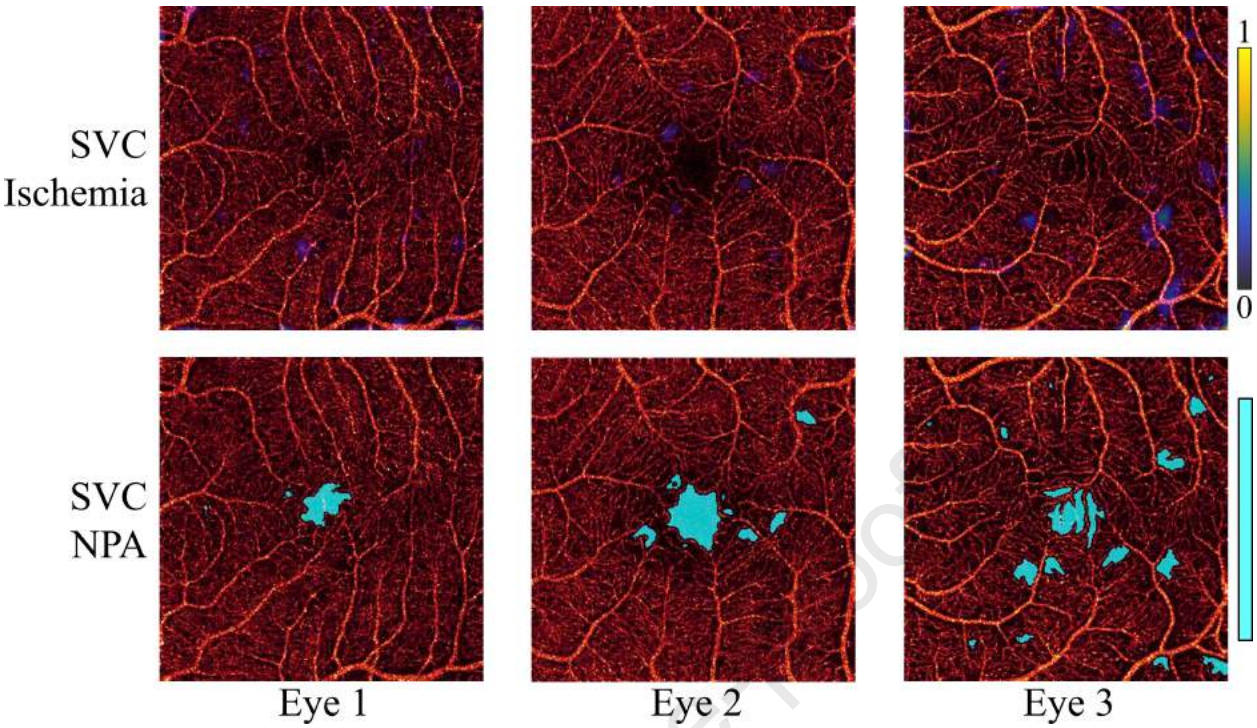

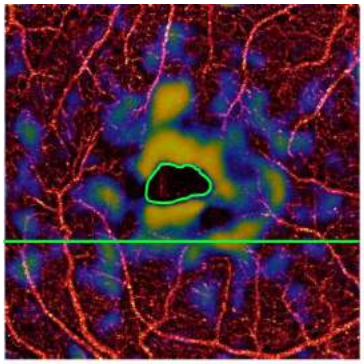

(A)

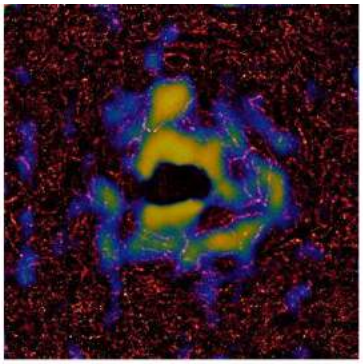

(B)

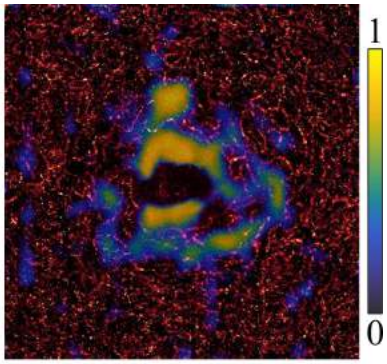

(C)

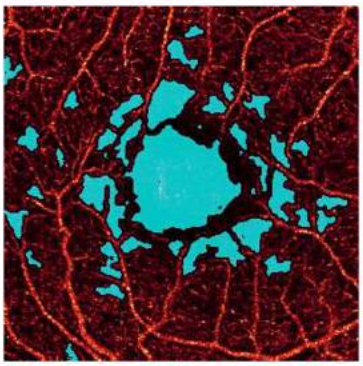

(D)

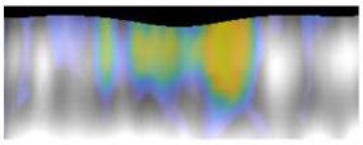

B-scan Oxygen tension

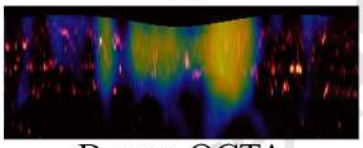

B-scan OCTA

(E)

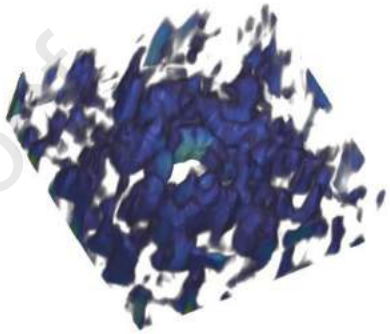

(F)

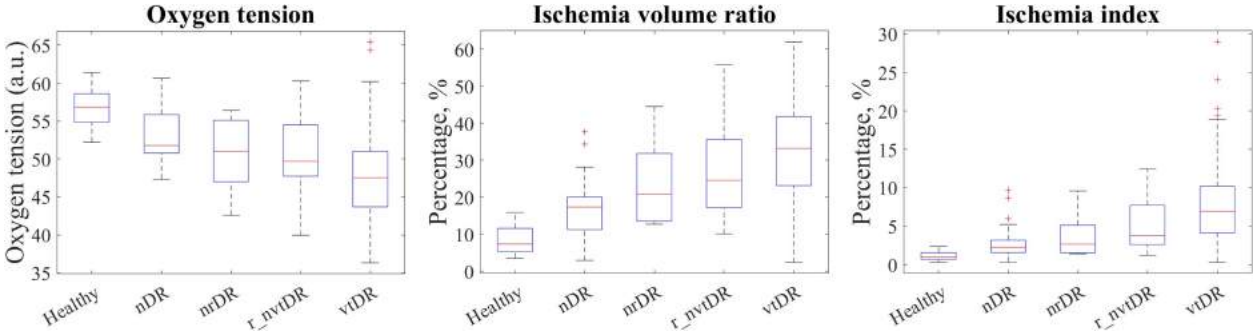

We proposed a three-dimensional quantitative analysis method for oxygen tension and ischemia using an oxygen diffusion model with zero-order kinetics based on skeletonized vasculature in volumetric optical coherence tomography angiography.